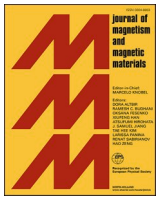
Journal of Magnetism and Magnetic Materials 630 (2025) 173415



Contents lists available at ScienceDirect

Journal of Magnetism and Magnetic Materials

journal homepage: www.elsevier.com/locate/jmmm



Research article

Analysis of magnetic domain evolution in rotational magnetization of GOES based on morphological characteristics and artificial neural network

Changgeng Zhang [a,b], Guotao Sun [a,b], Zhiwei Lin [a,b,c,*]

[a] State Key Laboratory of Intelligent Power Distribution Equipment and System, Hebei University of Technology, PR China
[b] Hebei Key Laboratory of Equipment and Technology Demonstration of Flexible DC Transmission, Hebei University of Technology, PR China
[c] Ningbo Magnetic Materials Application Technology Innovation Center Co., Ltd, Ningbo 315100 Zhejiang, PR China

ARTICLE INFO

Keywords:
Grain-oriented steel
Magneto-optical Kerr effect (MOKE)
Magnetic domains
Rotational magnetic field
Hu moments
artificial neural network (ANN)

ABSTRACT

Grain-oriented electrical steels (GOES) are widely used in power transformers due to their superior alternating magnetic properties. However, the mechanisms of rotational magnetization dominated in the T-section of transformer cores remain insufficiently explored and poorly predicted. Investigating the rotational magnetization of GOES from the perspective of magnetic domain morphology offers a novel and promising approach to address this research gap. In the study, the dynamic evolution of magnetic domains of grain-oriented electrical steel (GOES) under a rotational magnetic field are observed. Based on the shapes of these domains, the morphological parameters are extracted and analyzed from these domains, such as Hu moments. Subsequently, a full-connected neural network for predicting magnetization is trained using Hu moments as input features. The research results indicate that using morphological features as input data for neural network training and prediction is feasible and achieves high accuracy. In addition, through permutation feature importance (PFI) and ablation study, the parameter of Hu7 is identified as the main feature sensitive to rotational magnetization.

1. Introduction

Grain-oriented electrical steel (GOES) is a crucial soft magnetic material in the power industry, renowned for its exceptional magnetic properties, including low loss and high permeability[1,2]. Due to its superior alternating magnetic properties, grain-oriented steels are extensively used in transformer cores. However, in the T-section of three-phase transformers, the 2-D rotational magnetization prevails, resulting in more loss compared to alternating magnetization. The intrinsic magnetic characteristics of electrical steel under rotational magnetization differ significantly from those under 1-D alternating magnetization. Consequently, it is essential to investigate the intrinsic magnetic properties of electrical steel under 2-D magnetization [3].

The key to understanding this complex behavior lies in the material's microscopic magnetic domain structure. It is well-established that the dynamics of magnetic domains morphology are directly linked to macroscopic magnetic properties [4]. The influence of different types of magnetic domains on the hysteresis loop varies, including stripe domains and checkerboard domains observed under different stresses, as well as lancet domains resulting from misorientation[5]. Thus, observing and characterizing the magnetic domain structures of electrical steel is of great significance for high-fidelity hysteresis modeling.

The magneto-optical Kerr effect (MOKE) is an important physical phenomenon that involves changes in the polarization state of light under the influence of a magnetic field. This effect was first discovered by John Kerr and has been widely applied in subsequent research[6]. MOKE provides an effective tool for studying the magnetic properties of magnetic materials. By analyzing the changes in light reflection and transmission, researchers can obtain information about the magnetic state, magnetic field distribution, and microscopic magnetic domain structure of materials. In addition, MOKE has broad application potential in fields such as spintronics, magnetic storage devices, and nanotechnology [7,8]. With the development of materials science, the use of MOKE technology continues to evolve, making it an important means of understanding and utilizing the behavior of magnetic materials. It is possible to acquire magnetic domain images using MOKE and simultaneously measure the hysteresis loops. However, it is currently a challenge to establish a reliable relationship between domain images and hysteresis loops.

Regarding the qualitative relationship between magnetic domain structure and magnetization intensity, R. Schäfer from the Dresden

* Corresponding author.
E-mail address: jacklin7310@hotmail.com (Z. Lin).

https://doi.org/10.1016/j.jmmm.2025.173415
Received 18 March 2025; Received in revised form 10 July 2025; Accepted 1 August 2025
Available online 5 August 2025
0304-8853/© 2025 Elsevier B.V. All rights are reserved, including those for text and data mining, AI training, and similar technologies.

Institute conducted research on the magnetic domain structure of electrical steel. O. Perevertov observed and analyzed the magnetic domain structure and magnetic properties of grain oriented steel under in-plane compressive and tensile stresses [9,10]. The relationship between changes in magnetic domain structure and applied stress was summarized. Further analysis revealed that the stamping process leads to deterioration of magnetic domains near the stamping holes in grain-oriented silicon steel [11].

Morphological methods are effective for bridging the gap between magnetic domain morphology and quantitative analysis, especially in image processing and feature extraction. By utilizing computer vision technology, researchers have effectively identified and analyzed the morphology, structure, and dynamic characteristics of magnetic domains. These methods not only improve the efficiency of data processing, but also enhance the accuracy of analysis [12]. In the visualization process of magnetic domains, morphological techniques are widely used to generate high-quality images and 3-D reconstructions. For example, using image segmentation techniques, magnetic domains can be extracted from the background for further analysis. By applying edge detection algorithms, researchers can identify the boundaries of magnetic domains and quantify their morphological features [13]. In addition, morphological methods can also help simulate the dynamic changes of magnetic domains, providing important information about the behavior of magnetic materials under different external conditions [14]. For example, Foggiato used persistent homology (PH) combined with PCA to analyze magnetic domain images of nanocrystalline materials under different frequency magnetizations. They discovered the relationship between extracted variables and surface exchange energy [15]. and other studies have broadly used machine learning to predict properties of ferromagnetic materials [16,17].

Traditional approaches, such as interpreting dynamic magnetization based on observed trends in magnetic domain evolution or employing mathematical models to calculate macroscopic magnetic properties, are often limited to qualitative analysis or rely on overly idealized assumptions. However, artificial neural networks (ANNs) are particularly powerful in simulating complex nonlinear physical phenomena such as hysteresis [18]. Unlike traditional models, ANN is particularly suitable for directly learning the mapping from high-dimensional feature space to target output from experimental data, without the need for prior physical assumptions [19–21]. This ability makes it an ideal tool to bridge the final gap in our analysis chain.

In this paper, we examine magnetic domains on the surface of two silicon steel grains: one grain region is dominated by stripe domains, while the other one is characterized by lancet domains. We compare the optical signal changes of the two grains in a rotational magnetization state. Subsequently, Hu moments are calculated using morphological methods, and an artificial neural network is established to predict the light intensity reflected by MOKE. The results indicate that it is feasible to characterize magnetic domains by extracting features from morphology. In addition, through ablation studies and PFI analysis, it is found that descriptors related to rotation sensitivity are fed as inputs of the ANN model.

2. Methodology

The magnetic domain structures of oriented electrical steel under a specific magnetic field are identified using Canny edge detection. These structures are subsequently extracted to calculate Hu moments as their morphological features. Following this, an artificial neural network (ANN) is constructed to predict magnetization.

2.1. Canny edge detection and Hu moments

The fundamental principle of the Canny algorithm is to identify locations in an image where the intensity of gray levels exhibits the most significant changes[22–24]. The Sobel operator is used to calculate the gradients in the X direction (G_x) and Y direction (G_y), as well as the corresponding angles. Subsequently, the maximum gradient value and angle are computed (as shown in eq (1) and (2)) to delineate the boundary of domains.

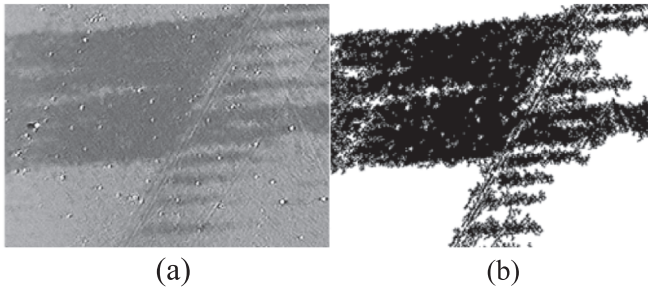


Fig. 1. (a) Original image, (b) processed image.

$$G = \sqrt{G_x^2 + G_y^2} \tag{1}$$

$$\theta = \arctan(\frac{G_x}{G_y}) \tag{2}$$

This methodology identifies the contours of magnetic domains to facilitate the subsequent extraction of domain shapes. The image initially undergoes filtering and binarization to enhance the intensity of gray-level variations.

Given the strong anisotropy of the oriented electrical steel in the rolling direction, it can be assumed that the magnetic domains are all 180° strip domains. Therefore, this processing process is reasonable, and the result is shown in Fig. 1.

The parameter Q of oriented steel is much smaller than 1, so that its magnetic moment can be considered in-plane[1]. The parameter Q is calculated as follows:

$$Q = K/K_d \tag{3}$$

$$K_d = J_s^2/2\mu_0 \tag{4}$$

where K_d represents the material parameter, K denotes the anisotropy coefficient, μ_0 is the vacuum permeability, and J_s stands for the saturation magnetization. For silicon steel, $J_s = 1.8$T, and K is given by eq.(5), with units of ergs/cc[25]:

$$K = 4.77 - 0.21256 \times [\text{at.\% Si}] - 0.03816 \times [\text{at.\% Al}] \tag{5}$$

where at.% denotes the atomic weight fraction of the element.

Hu moments constitute a set of seven invariant moments extensively utilized in image analysis [26]. These moments are derived from the geometric moments of two-dimensional images and exhibit invariance to translation, rotation, and scaling. Consequently, for images of identical objects, irrespective of their position, size, or orientation, the calculated Hu moments remain consistent[27,28]. These properties render Hu moments particularly suitable for capturing the intrinsic morphological characteristics of magnetic domains, such as aspect ratio, edge complexity, and symmetry.

The (p,q) order central moment of a shape is defined as:

$$\mu_{pq} = \sum_x \sum_y (x - \bar{x})^p (y - \bar{y})^q I(x,y) \tag{6}$$

Where $I(x,y)$ is the pixel value at the coordinates (x,y) in the image, and $(\bar{x},\bar{y})$ are the coordinates of the image's centroid, where $\bar{x} = m_{10}/m_{00}$, $\bar{y} = m_{01}/m_{00}$, m_{pq} is the (p, q)-th raw moment of the image, with the calculation formula as shown in eq (7):

$$m_{pq} = \sum_x \sum_y x^p y^q I(x,y) \tag{7}$$

Table 1
Hu moments and its morphological meaning.

Hu Moment Parameter	Morphological Meaning
Hu 1	Overall area or energy
Hu 2	Aspect ratio and elongation
Hu 3	Symmetry between axes, rotation-sensitive
Hu 4	Concavity and local detail detection
Hu 5	Planar curvature changes, noise-robust
Hu 6	Shape asymmetry and complex curvature.
Hu 7	Curvature and sharp features, rotation-sensitive.

By normalizing these central moments, the normalized central moments are obtained:

$$\eta_{pq} = \frac{\mu_{pq}}{\mu_{00}^{\gamma}} \tag{8}$$

where $\gamma = 1+(p+q)/2$.

The Hu moments are calculated using these normalized central moments:

$$\begin{cases} C_1 = \eta_{10} + \eta_{20} \\ C_2 = (\eta_{20} - \eta_{02})^2 + 4\eta_{11}^2 \\ C_3 = (\eta_{30} - 3\eta_{12})^2 + (3\eta_{21} - \eta_{03})^2 \\ C_4 = (\eta_{30} + \eta_{12})^2 + (3\eta_{21} + \eta_{03})^2 \\ C_5 = (\eta_{30} - 3\eta_{12})(\eta_{30} + \eta_{12})[(\eta_{30} + \eta_{12})^2 - 3(\eta_{21} + \eta_{03})^2] \\ \quad +(3\eta_{21} - \eta_{03})[(\eta_{30} + \eta_{12})^2 - (\eta_{21} + \eta_{03})^2] \\ C_6 = (\eta_{20} - \eta_{02})[(\eta_{30} + \eta_{12})^2 - (\eta_{21} + \eta_{03})^2] \\ \quad +4\eta_{11}[(\eta_{30} + \eta_{12})^2 - (\eta_{21} + \eta_{03})^2] \\ C_7 = (\eta_{20} + \eta_{02})[(\eta_{30} + \eta_{12})^2 - (\eta_{21} + \eta_{03})^2] \\ \quad -4\eta_{11}[(\eta_{30} + \eta_{12})^2 - (\eta_{21} + \eta_{03})^2] \end{cases} \tag{9}$$

where η_{ij} denotes the (i,j)-th order normalized central moment.

The seven parameters of Hu moments are dimensionless invariant moments used to describe the shape features of images. The specific morphological meanings of each parameter are shown in Table 1[28]:

2.2. ANN

Artificial Neural Networks (ANNs) consist of interconnected neurons designed to train complex data patterns. A dense neural network is employed to process the high-dimensional input data, enabling efficient learning from the complex magnetic domain morphology represented as:

$$y = f(\boldsymbol{W}x + b) \tag{10}$$

where y represents the output of the network, $\mathbf{W}$ denotes the weight matrix, x is the input vector, consisting of 7 Hu moments, and b is the bias. The activation function f, specifically the Rectified Linear Unit (ReLU), mitigates the vanishing gradient problem and improves training performance. The ReLU function is expressed as:

$$f(x) = \max(0, x) \tag{11}$$

where $f(x)$ represents the output of the activation function, while x denotes the input to the function. This non-linear activation allows the network to capture complex data relationships, enhancing predictive performance. The dense neural network leverages this capability to model intricate patterns in the input data, improving prediction accuracy.

The specific architecture and hyperparameters for our model are selected using a pragmatic and focused approach to ensure both effectiveness and reproducibility. We established a strong baseline architecture consisting of two hidden layers with 10 and 8 neurons, respectively, which initial explorations showed was sufficient for the complexity of our problem.

Table 2
Hyperparameters for the ANN Model.

Hyperparameter	Value
Input Layer Neurons	7
Hidden Layers	2
First Hidden Layer Neurons	10
Second Hidden Layer Neurons	8
Output Layer Neurons	1
Activation Function	ReLU
Optimizer	Adam
Learning Rate	0.001
Loss Function	MSE
Training Epochs	200
Batch Size	16

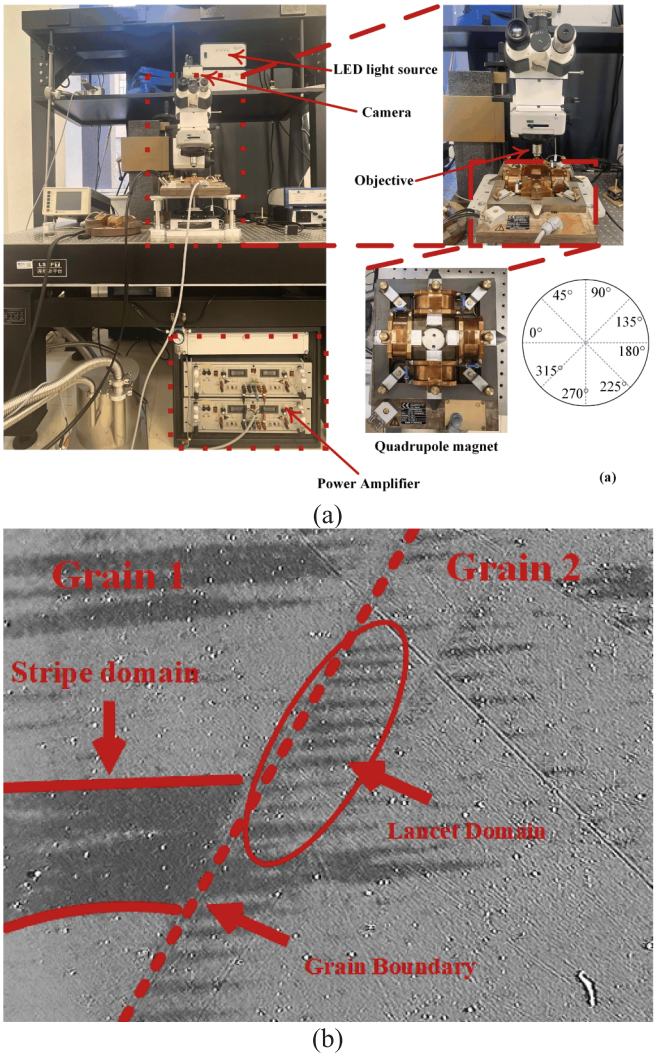


Fig. 2. (a) MOKE Microscope, (b) MOKE image of the selected analysis area, showing Grain 1 (left, dominated by stripe domains) and Grain 2 (right, dominated by lancet domains).

The training process is carefully controlled to achieve convergence without overfitting. The Adam optimizer is chosen with a standard learning rate of 0.001, while the Mean Squared Error (MSE) is chosen as the loss function. The model is trained for 200 epochs with a batch size of 16, a configuration that allowed the validation loss to stabilize,

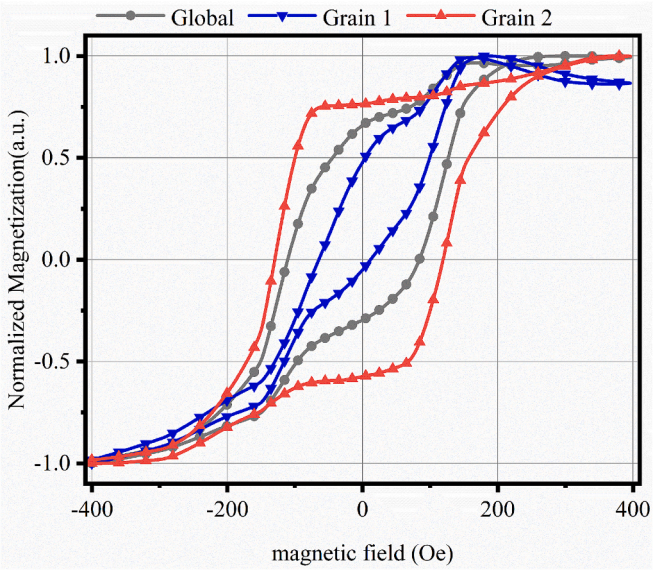


Fig. 3. Kerr signal and magnetic hysteresis loop under one-dimensional quasi-static condition.

indicating that the model had learned the underlying patterns effectively. The hyperparameters are summarized in Table 2.

3. Experimental

In this study, magnetic domain imaging was conducted using a MOKE microscope (Evico, Germany), as depicted in Fig. 2(a). The setup was configured with s-polarized light to primarily detect the longitudinal Kerr effect. The sample under investigation is a high-induction grain-oriented electrical steel (B30P120, Baosteel). The observation area, shown in Fig. 2(b), was specifically chosen to include two adjacent grains with distinct magnetic domain structures under quasi-static conditions. The left grain (Grain 1) is dominated by 180° stripe domains, while the right grain (Grain 2) exhibits more complex lancet domains. These structures are typical in oriented steels, arising from local internal stress and slight crystallographic misorientations. By capturing the behavior of these different domain types simultaneously, we aim to generate a comprehensive dataset to train and validate a neural network model, enhancing its versatility and robustness.

According to Ref. [29], due to the Kerr effect, the reflected light intensity of a magnetized surface in a plane depends on the direction of surface magnetization, as shown in eq. (12):

$$I = I_0 + Am_l + Bm_t + C \tag{12}$$

where A, and B are scale factors, and C is the contribution of the square of the magnetic moment to the intensity. The m_l and m_t are longitudinal and transverse magnetic moment components. I_0 is a reflection constant related to normal light amplitudes N. A and B are both related to the product of reflection coefficient N and Kerr amplitudes K_i ($i = l,t$). C is related to the square of Kerr amplitudes K_i. Due to the absence of transverse Kerr effect in s-polarized light, the contribution of m_t to intensity is zero and since N is much larger than K_i, the contribution of C in intensity can be ignored. So the intensity I can be regarded as having a linear relationship with the longitudinal magnetization m_l,as shown in Fig. 3.

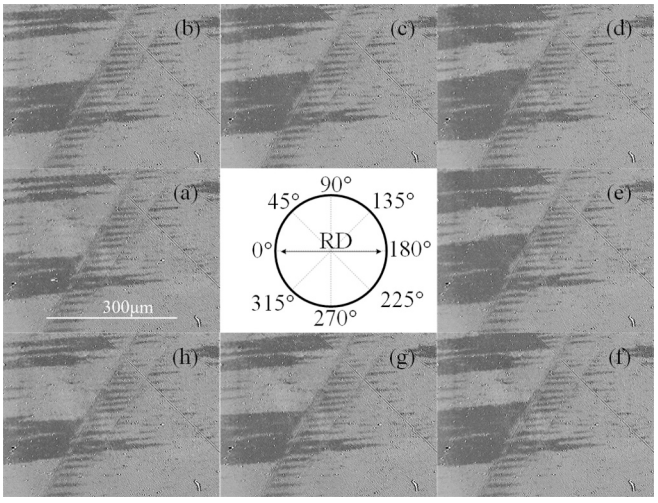


Fig. 5. Domain image under 20Oe rotational magnetic field: (a) 0° (b) 45° (c) 90° (d) 135° (e) 180° (f) 225° (g) 270° (h) 315°.

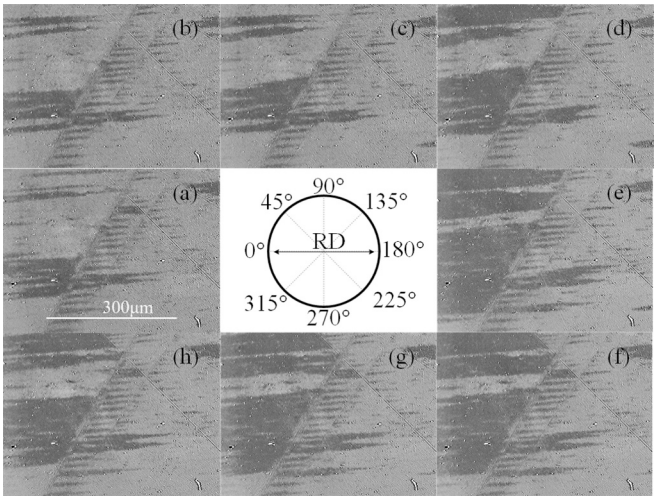


Fig. 6. Domain image under 50Oe rotational magnetic field: (a) 0° (b) 45° (c) 90° (d) 135° (e) 180° (f) 225° (g) 270° (h) 315°.

To characterize the fundamental magnetic properties of the selected area, a 1-D quasi-static magnetization cycle was first applied along the sample's rolling direction (RD). The magnetic field measured by the MOKE microscope and the intensity curve of the Kerr signal of two grains and the global Kerr signal are shown in Fig. 3. The y-axis has been normalized from intensity to −1 to 1 to characterize magnetization. The domain images corresponding to the rising edge curve from −400 Oe to 400 Oe are shown in Fig. 4. It can be observed that due to the pinning effect and asymmetric loops, the coercive force of grain 1 dominated by stripe domains is lower than that of grain 2 dominated by lancet domains. It shows that lancet domains serve as more effective pinning sites, creating higher energy barriers that impede domain wall motion and

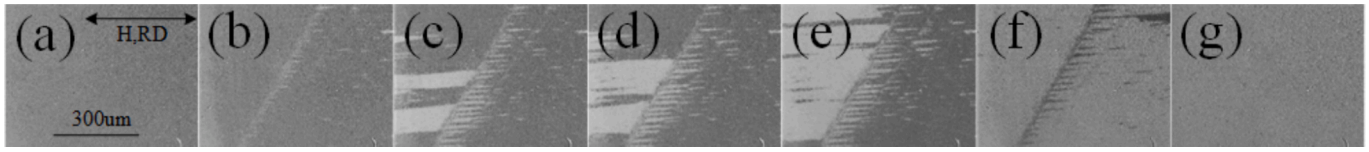


Fig. 4. Domain images under 1D magnetic field: (a) −400Oe, (b) −200Oe, (c) −100Oe, (d) 0Oe, (e) 100Oe, (f) 200Oe, (g) 400Oe.

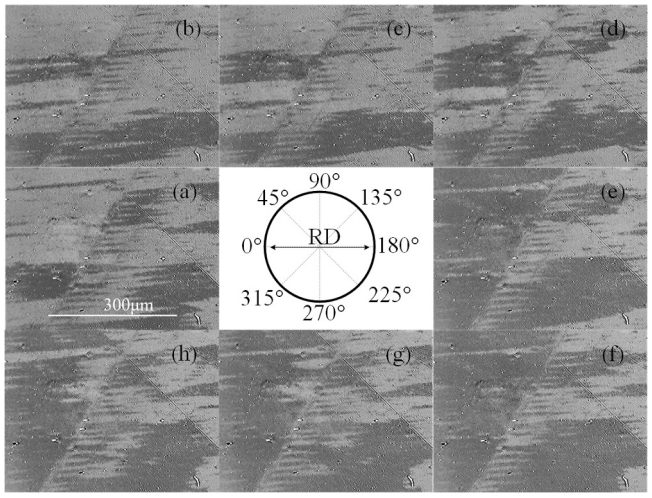


Fig. 7. Domain image under 100Oe rotational magnetic field: (a) 0° (b) 45° (c) 90° (d) 135° (e) 180° (f) 225° (g) 270° (h) 315°.

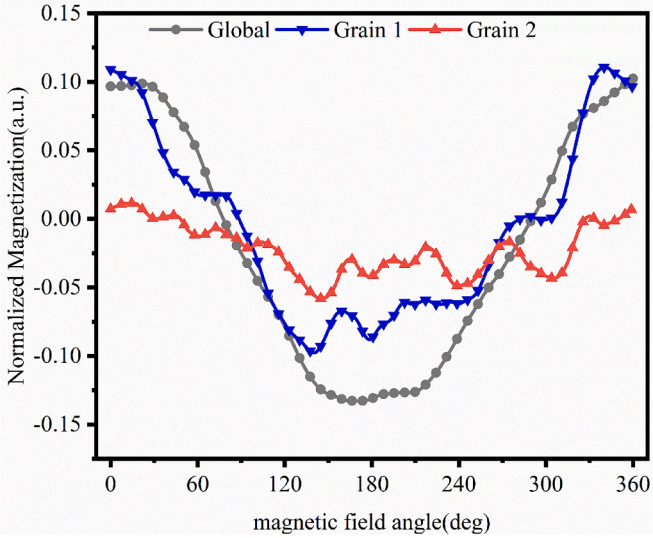


Fig. 8. The relationship between intensity and excitation degree under a rotating magnetic field of 20Oe.

magnetization reversal. At 200Oe, there are no more complex magnetic domain structures in the region with domain walls disappeared, entering the stage of magnetic moment rotation.

Based on the results of one-dimensional experiments, apply a rotating magnetic field of 20-100Oe on the silicon steel sample. According to Figs. 3 and 4, the sample at 200Oe has not shown the magnetic domain pattern and approached saturation, where the translational motion of the magnetic domain walls disappeared and the rotational motion occurred.

The magnetic domain images of rotational magnetic fields at 20/50/100Oe are shown in Figs. 5-7. Since the points under 20 Oe and 50 Oe are very close in Fig. 3, there is no significant difference in the morphology of magnetic domains under rotational magnetization.

The intensity under 20/50/100Oe rotational magnetization is shown in Figs. 8-10. Due to the irreversible displacement of magnetic domain walls, there is a difference in magnetization intensity before and after one rotation of the magnetic field. Magnetic domain images will be used to calculate morphological features as input to the network, and intensity will be used as labels for ANN network modeling.

Ideally, the intensity is expected to attain its maximum and

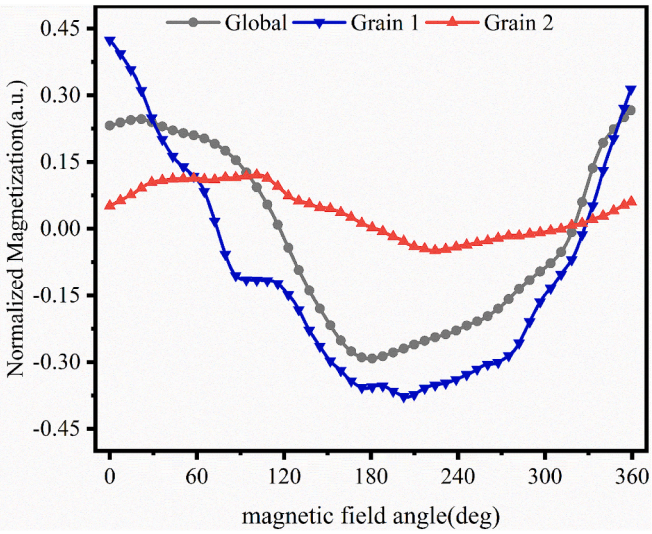


Fig. 9. The relationship between intensity and excitation degree under a rotating magnetic field of 50Oe.

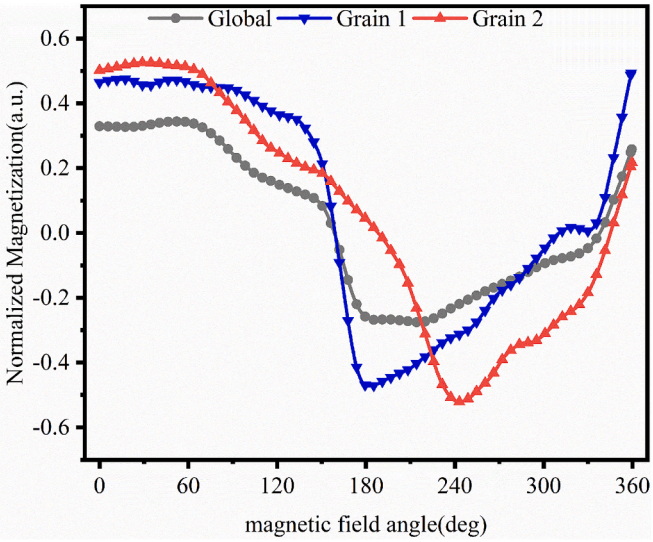


Fig. 10. The relationship between intensity and excitation degree under a rotating magnetic field of 100Oe.

minimum values at 0° and 180°, respectively, reflecting the positive and negative peak magnetizations. However, due to the large grain sizes of the oriented steel, global observations are challenging. In addition, the pinning effect on the surface and observation area can lead to deviation from this ideal state, which is also the difference between local and global magnetization.

4. Results and discussion

4.1. Magnetic domain dynamics and their impact on magnetization

The magnetic behavior of grain-oriented electrical steel is governed by its complex, three-dimensional domain structure. Consequently, the magnetic properties observed at the surface via MOKE, while not identical to the bulk response, serve as an indispensable proxy that reflects underlying bulk mechanisms. Understanding the nuances of this surface-to-bulk relationship is critical, and it begins with a detailed analysis of the surface domain morphology and its direct impact on magnetization.

This fundamental difference in domain stability persists and becomes

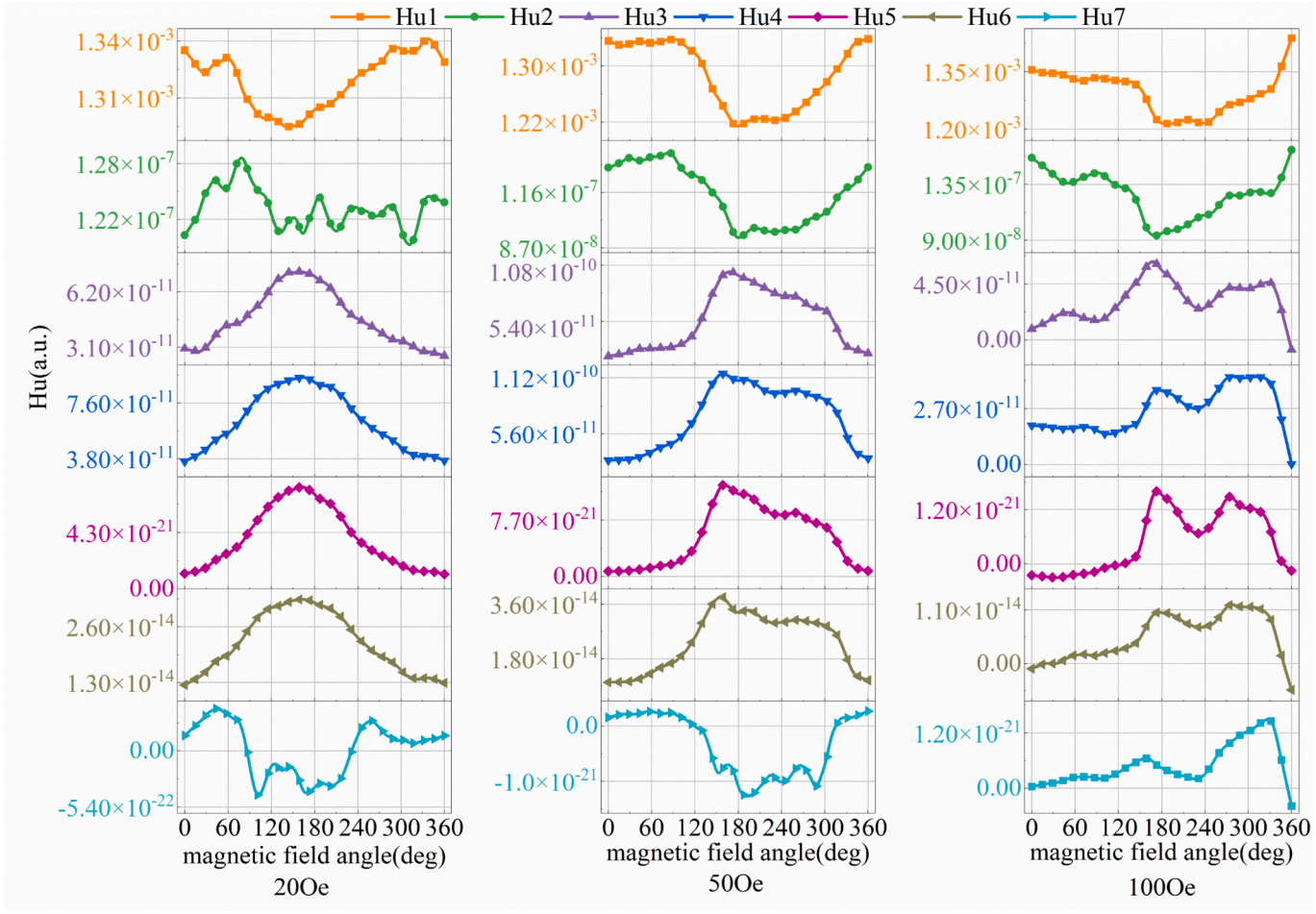


Fig. 11. The relationship between Hu moment and excitation angle under different amplitudes.

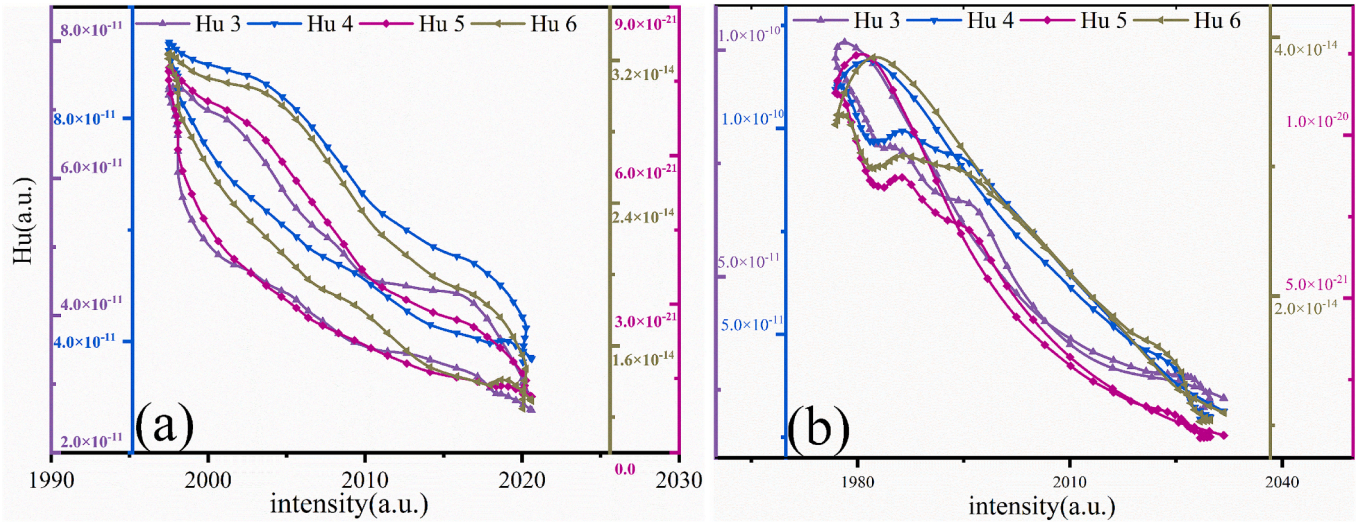


Fig. 12. The relationship between Hu3 ~ 6 and intensity: (a) 20Oe, (b) 50Oe.

more complex under rotational fields. At low to medium field strengths (20 and 50 Oe), the magnetization response of Grain 2 is more hysteretic (Figs. 8-9). This macroscopic behavior corresponds directly to the microscopic observations (Figs. 5-6), where its stable lancet domains undergo less drastic rearrangement compared to the more mobile stripe domains in Grain 1. Conversely, at a higher field of 100 Oe, some lancet domains begin to break down and transform into simpler, stripe-like patterns. This morphological transition correlates with a sharper increase in magnetization, as the pinning effect weakens.Fig. 10..

Collectively, these observations highlight that the material magnetization is inextricably linked to its local domain morphology. This close relation supports our quantitative, feature-based approach for predictive

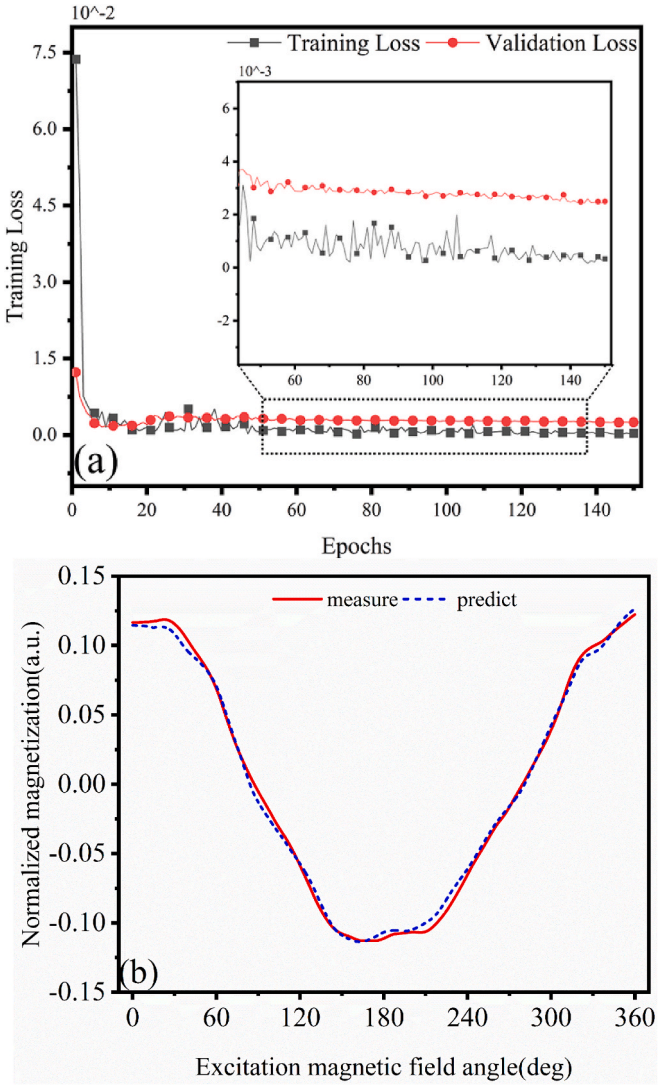


Fig. 13. Training loss curve (a) and prediction results (b) under rotational magnetization.

modeling.

4.2. Hu moments of magnetic domains

The Hu moments of magnetic domain images with different amplitude rotational field are presented in Fig. 11. While the values differ across field strengths, certain trends are consistent: Hu3–Hu6 remain stable in low and medium fields, whereas Hu1 and Hu2 display similar variations at high field amplitudes.

As shown in Fig. 12, the curves of Hu3 ~ 6 versus intensity at 20 and 50Oe are presented. At 20 Oe and 50 Oe, the values of Hu3 to Hu6 are almost linearly proportional to magnetization.

4.3. Magnetization prediction by ANN

An Artificial Neural Network (ANN) is developed to predict magnetization from morphological features. The model, composed of two fully connected hidden layers, is trained using Hu moment data from the 50 Oe and 100 Oe experiments, with the measured Kerr intensity serving as the training label. The dataset excited by 20Oe is reserved for validation.

The model's performance is shown in Fig. 13. The predicted magnetization shows a good agreement with the measured values, confirming the feasibility of the proposed method.

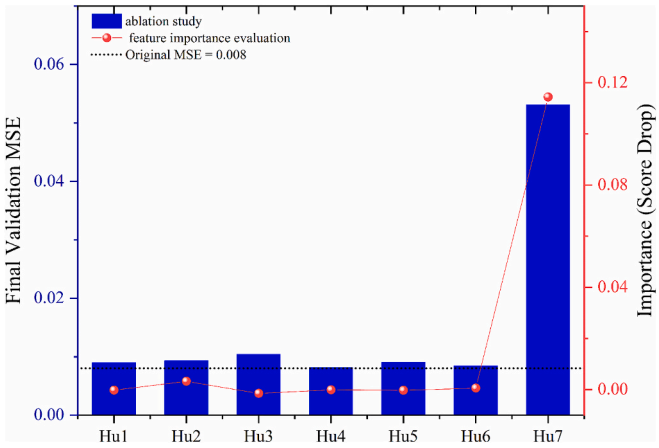


Fig. 14. Dual analysis of feature importance. The bar chart shows the model's validation MSE after the removal of each Hu moment (ablation study). The line plot shows the importance score for each feature (permutation feature importance).

4.4. Ablation study and permutation feature importance

A critical test for our ANN model is to verify that it learns underlying physical relationships rather than merely interpolating the training data. To interpret the model's mechanism, we perform a dual analysis using a Systematic Ablation Study and Permutation Feature Importance (PFI).

The results of this analysis, presented in Fig. 14, unequivocally identify the seventh Hu moment (Hu7) as the dominant predictor of the magnetization state. In the ablation study, removing Hu7 increased the validation MSE nearly seven-fold (from 0.0080 to 0.0531). Similarly, its PFI score (0.11446) was orders of magnitude greater than that of any other feature. This finding is physically intuitive: Hu7 is sensitive to rotational symmetry, and as a result, also sensitive to rotational magnetization. It demonstrates that the most critical morphological signature Hu7 of the process is identified.

Furthermore, the analysis reveals complex, non-trivial feature interactions. For instance, Hu3 shows a negative PFI score, yet its removal still harms model performance. This indicates that Hu3 interacts synergistically with other features, helping the model to better interpret the overall domain structure.

4.5. Physical Interpretation of Hu moments

Hu moments are powerful shape descriptors that are invariant to translation, scaling, and rotation, which provide quantitative features of the geometric and topological characteristics of magnetic domain structures. For example, Hu1 and Hu2 are quantities related to the overall size and elongation of magnetic domains, and their changes can reflect the growth or contraction of strip-shaped domains; Higher order Hu moments (Hu3-Hu7) capture more complex shape details. Although the individual physical roles of Hu3-Hu7 are more abstract, their collective changes provide high-dimensional features for complex events such as domain wall pinning or topological switching, which cannot be captured solely through simple metrics such as domain area.

The proposed ANN model learns complex nonlinear relationships between all seven moments and magnetization. This enables the model to identify subtle but significant dynamic changes in the domain morphology under rotational magnetization.

5. Conclusion

In this paper, the variations of magnetic domains under excitation of rotational fields with different amplitudes are captured by magneto-optic Kerr microscopy. Subsequently, the changes in Hu moments are

extracted through morphological analysis methods for further examination. These Hu moment data are then employed as input features for training an artificial neural network (ANN).

(1) The results of Hu moments reveal a correlation among specific Hu moment values in the rotational magnetization state. Notably, the trends of Hu3 to Hu6 are consistent under low to medium rotating magnetic fields. Additionally, an association exists between Hu moments and light intensity (magnetization), with Hu3 to Hu6 showing a relationship to magnetization specifically in low to medium rotating magnetic fields.
(2) The ANN results indicate that modeling magnetization from morphological features is a feasible approach. Crucially, a feature importance analysis revealed that the model learned physically meaningful relationships, identifying the 7th Hu moment (related to rotational distortion) as the key predictor.

CRediT authorship contribution statement

Changgeng Zhang: Data curation, Formal analysis, Funding acquisition, Resources, Software, Supervision. **Guotao Sun:** Writing – original draft, Investigation, Validation, Visualization. **Zhiwei Lin:** Writing – review & editing, Conceptualization, Methodology, Funding acquisition.

Declaration of competing interest

The authors declare that they have no known competing financial interests or personal relationships that could have appeared to influence the work reported in this paper.

Acknowledgments

This work was supported in part by the National Key R&D Program of China [No. 2023YFB3809200], the National Natural Science Foundation of China, (No. 52277008), and Natural Sciences foundation of Hebei Province, China (E2023202050).

Data availability

The data that has been used is confidential.

References

[1] Hubert A, Schäfer R. Magnetic domains: the analysis of magnetic microstructures [M].Berlin: Springer, 2008.
[2] K. Iwata, S. Arai, K. Ishiyama, Calculation of basic domain width considering lancet domains in (110)[001]Fe3%Si, IEEE Trans. Magn. 50 (2) (2014) 353–356.
[3] C. Zhang, Y. Li, J. Li, et al., Measurement of three-dimensional magnetic properties with feedback control and harmonic compensation, IEEE Trans. Ind. Electron. 64 (3) (2016) 2476–2485.
[4] Suwas S, Ray R K. Crystallographic texture of materials[M]. London: Springer, 2014.
[5] K. Iwata, M. Suzuki, M. Hashimoto, et al., Temperature dependence of lancet domains in grain-oriented Fe-3% Si steels, IEEE Trans. Magn. 51 (11) (2015) 1–4.
[6] M. Mansuripur, The magneto-optical Kerr effect, Optics and Photonics News 11 (10) (2000) 34.
[7] J.Y. Bigot, N. Van Huylenbroeck, Magneto-Optical Effects in magnetic Materials: applications and prospects, Phys. Rev. Lett. 87 (12) (2001) 127203.
[8] X. Zhang, Y. Liu, Spintronics: from Fundamentals to applications, Nat. Rev. Mater. 1 (3) (2014) 14004.
[9] O. Perevertov, R. Schäfer, Influence of applied tensile stress on the hysteresis curve and magnetic domain structure of grain-oriented Fe–3% Si steel, J. Phys. D Appl. Phys. 47 (18) (2014) 185001.
[10] O. Perevertov, R. Schäfer, Magnetic properties and magnetic domain structure of grain-oriented Fe-3% Si steel under compression, Mater. Res. Express 3 (9) (2016) 096103.
[11] T. Gunes, R. Schäfer, N. Derebasi, Quantitative analysis of magnetic field distribution around circular non-magnetic region in grain-oriented Fe-3% Si steel, IEEE Trans. Magn. 54 (2) (2017) 1–8.
[12] De Gennes P G, Prost J. The physics of liquid crystals[M]. Oxford university press, 1993.
[13] K.A. Hunnestad, E.D. Roede, A.T.J. van Helvoort, et al., Characterization of ferroelectric domain walls by scanning electron microscopy, J. Appl. Phys. 128 (19) (2020).
[14] S.E. Russek, W.E. Bailey, Magnetic domain structure and imaging of Co-Pt multilayer thin-film nanostructures, IEEE Trans. Magn. 36 (5) (2000) 2990–2992.
[15] A.L. Foggiatto, R. Nagaoka, M. Taniwaki, et al., Analysis of the excess loss in high-frequency magnetization process through machine learning and topological data analysis, IEEE Trans. Magn. (2024).
[16] G.L.W. Hart, T. Mueller, C. Toher, et al., Machine learning for alloys, Nat. Rev. Mater. 6 (8) (2021) 730–755.
[17] Q. Fu, Y.H. Sha, F. Zhang, et al., Correlative effect of critical parameters for η recrystallization texture development in rolled Fe81Ga19 sheet: Modeling and experiment, Acta Mater. 167 (2019) 167–180.
[18] Z. Zhao, F. Liu, S. L. Ho, W. N. Fu and W. Yan, "Modeling Magnetic Hysteresis Under DC-Biased Magnetization Using the Neural Network," in IEEE Transactions on Magnetics, vol. 45, no. 10, pp. 3958-3961.
[19] T. Xie, J.C. Grossman, Crystal graph convolutional neural networks for an accurate and interpretable prediction of material properties, Phys. Rev. Lett. 120 (14) (2018) 145301.
[20] A. Agrawal, A. Choudhary, Perspective: Materials informatics and big data: Realization of the "fourth paradigm" of science in materials science, APL Mater. 4 (5) (2016).
[21] T. Lookman, P.V. Balachandran, D. Xue, R. Yuan, Active learning in materials science with emphasis on adaptive sampling using uncertaintyes for targeted design, npj Comput. Mater. 5 (1) (2019) 21.
[22] R. Song, Z. Zhang, H. Liu, Edge connection based Canny edge detection algorithm, Pattern Recognit Image Anal. 27 (2017) 740–747.
[23] M. Baştan, S.S. Bukhari, T. Breuel, Active Canny: edge detection and recovery with open active contour models, IET Image Proc. 11 (12) (2017) 1325–1332.
[24] J. Canny, A computational approach to edge detection, IEEE Trans. Pattern Anal. Mach. Intell. 6 (1986) 679–698.
[25] C. Kittel, Physical theory of ferromagnetic domains, Usp. Fiz. Nauk 41 (4) (1950) 452–544.
[26] M.K. Hu, Visual pattern recognition by moment invariants, IRE Trans. Inf. Theory 8 (2) (1962) 179–187.
[27] D. Žunić, J. Žunić, Shape ellipticity from Hu moment invariants, Appl. Math Comput. 226 (2014) 406–414.
[28] Flusser J, Zitova B, Suk T. Moments and moment invariants in pattern recognition [M]. John Wiley & Sons, 2009.
[29] I.V. Soldatov, R. Schäfer, Advances in quantitative Kerr microscopy, Phys. Rev. B 95 (1) (2017) 014426.